BIOCATALYSIS

Directed evolution of nonheme iron enzymes to access abiological radical-relay C(sp³)-H azidation

Jinyan Rui¹†, Qun Zhao¹†, Anthony J. Huls¹†, Jordi Soler², Jared C. Paris³, Zhenhong Chen¹, Viktor Reshetnikov¹, Yunfang Yang⁴, Yisong Guo³*, Marc Garcia-Borràs²*, Xiongyi Huang¹*

We report the reprogramming of nonheme iron enzymes to catalyze an abiological $C(sp^3)$ –H azidation reaction through iron-catalyzed radical relay. This biocatalytic transformation uses amidyl radicals as hydrogen atom abstractors and Fe(III)– N_3 intermediates as radical trapping agents. We established a high-throughput screening platform based on click chemistry for rapid evolution of the catalytic performance of identified enzymes. The final optimized variants deliver a range of azidation products with up to 10,600 total turnovers and 93% enantiomeric excess. Given the prevalence of radical relay reactions in organic synthesis and the diversity of nonheme iron enzymes, we envision that this discovery will stimulate future development of metalloenzyme catalysts for synthetically useful transformations unexplored by natural evolution.

ntroducing abiological chemical transformations to natural proteins represents a powerful approach to advance enzymatic catalysis to reaction territories unexplored by natural evolution (1). This strategy enables enzyme reprogramming to achieve challenging synthetic reactions regio- and enantioselectively while maintaining genetic tunability (2, 3). Representative examples include taming heme and nonheme metalloenzymes

to mediate carbene- and nitrene-transfer reactions (4), reprogramming flavoenzymes for photoredox catalysis (5, 6), and reconfiguring carbonic anhydrase to perform metal-hydride chemistry (7). Despite this progress, most reactions in organic synthesis have no known biological counterparts, and the mechanisms that empower these transformations were not developed by nature during the course of natural evolution (I). To unleash the full potential

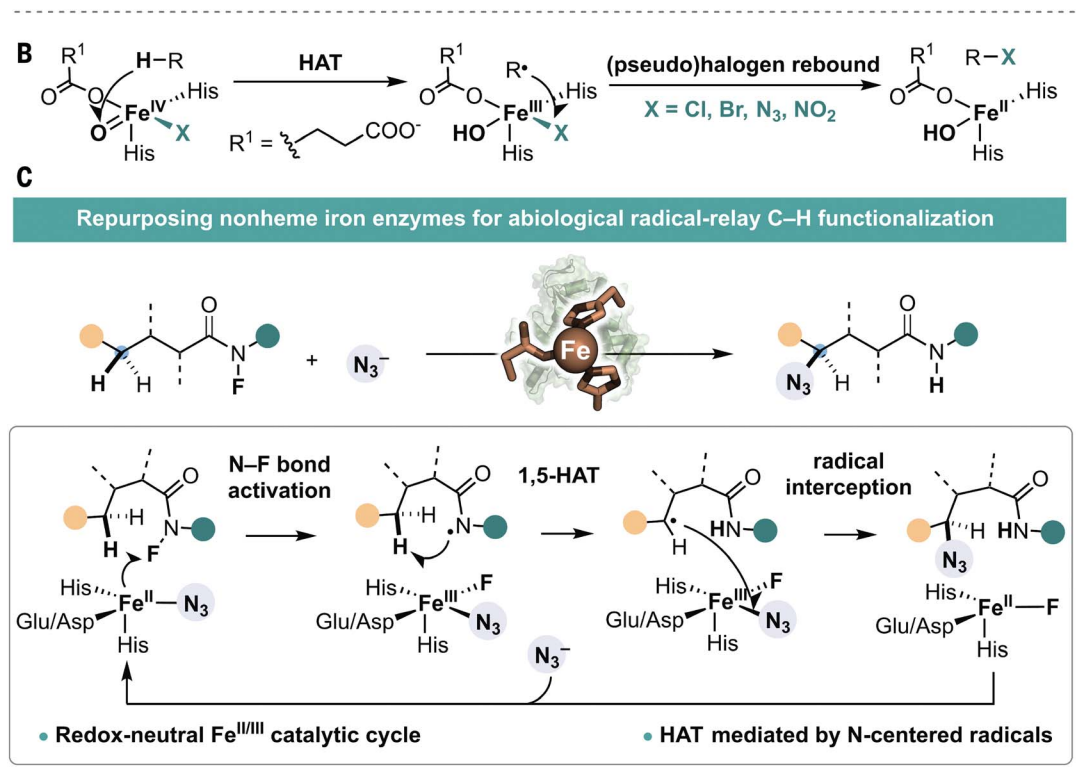
hydrogen atom transfer

of enzymes for modern chemical synthesis, it is pivotal to introduce fundamental reaction modes in synthetic chemistry to the catalytic repertoire of biology.

We consider a mechanism-driven approach to expand the scope of biocatalysis. We envisioned that natural metalloenzymes that share mechanistic elements with synthetic metal-catalyzed reactions would exhibit promiscuous activity toward these reactions, from which new catalvtic functions can be evolved. Guided by this design principle, we envisaged that nonheme iron enzymes could be reprogrammed to perform radical-relay C-H functionalization—an important class of unnatural reactions widely used in organic synthesis (8-11). The defining feature of a metal-catalyzed radical relay is the use of a reactive radical (X•) to activate a C(sp³)-H bond through hydrogen atom transfer (HAT) and the interception of the resulting carbon-centered radical by a redox-

Department of Chemistry, Johns Hopkins University, Baltimore, MD 21218, USA. Institut de Química Computacional i Catàlisi (IQCC) and Departament de Química, Universitat de Girona, Campus Montilivi, Girona E-17071 Catalonia, Spain. Department of Chemistry, Carnegie Mellon University, Pittsburgh, PA 15213, USA. College of Chemical Enginering, Zhejiang University of Technology, Hangzhou, Zhejiang 310014, China. Corresponding author. Email: xiongyi@jhu.edu (X.H.); marc.garcia@udg.edu (M.G.B.); ysguo@andrew.cmu.edu (Y.G.) iThese authors contributed equally to this work.

Fig. 1. Conceptualization of enzymatic C-H functionalization via metal-catalyzed radical relay. (A) Radical-relay C-H functionalization involves an initial hydrogen atom transfer (HAT) mediated by a heteroatomcentered radical (X•) followed by trapping of the carbon-centered radical with a redox-active metal complex. (B) Mechanism employed by natural nonheme iron enzymes for C(sp³)-H halogenation/azidation. (C) Integration of radical relay chemistry into nonheme iron enzymes enables unnatural C-H functionalization reactions.



Rui et al., Science **376**, 869-874 (2022) 20 May 2022 **1 of 6**

active metal complex (Fig. 1A). This process mechanistically resembles the C(sp³)-H halogenation reactions catalyzed by nonheme iron halogenases, in which an iron(IV)-oxo complex is used to activate substrates by means of HAT and an iron(III)halide/azide intermediate intercepts substrate radicals to form carbon-halogen/azide bonds (Fig. 1B) (12-16). Enlightened by this mechanistic similarity, we proposed that a nonheme iron enzyme could mediate a radical relay process through an initial substrate activation at a Fe(II) center to generate a reactive amidyl radical for HAT and subsequent transfer of a Fe(III)-bound ligand to the carbon-centered radical (Fig. 1C). This new biocatalytic reaction proceeds through a redox neutral pathway involving an Fe^{II}/Fe^{III} redox couple, which offers a complementary approach to the native Fe^{II/IV} catalytic cycle of nonheme iron enzymes for C-H functionalization.

As proof-of-concept, we employed this enzymatic radical-relay strategy to develop new biocatalysts to perform a nonnatural C(sp³)–H azidation reaction. Current synthetic approaches for this reaction are limited in turnovers, not enantioselective, and require an acidic azide source (scheme S4) (17). We presumed that these challenges could be met by leveraging

the genetic tunability and high catalytic efficiency of nonheme iron enzymes. We began our investigation by testing a panel of nine functionally diverse nonheme iron enzymes with an N-fluoroamide substrate 1NF under wholecell conditions. A (4-hydroxyphenyl)pyruvate dioxygenase from Streptomyces avermitilis (Sav HppD) provided the desired azidation product with 250 total turnovers (TTN), an enantiomeric ratio (e.r.) of 63:37, and a chemoselectivity of 9:1 for azidation over fluorination product (tables S1 and S2). Only a trace amount of the azidation product was obtained in a reaction lacking Sav HppD entry 10, table S1. Moreover, mutating the two iron-coordinating histidines to alanines abolished the enzyme activity while retaining the fold of wild-type (WT) Sav HppD (entry 11, table S1, and fig. S1), supporting the proposal that this enzymatic azidation occurs at the 2-His-1-carboxylate iron center. The unazidated amide product was also detected in trace amounts but was likely formed through an unidentified nonenzymatic process as the double alanine mutant afforded this product in a yield comparable to that of the WT enzyme (tables S1 and S2).

We set out to improve the performance of *Sav* HppD through directed evolution. We performed computational modeling on the

WT enzyme with both azide and 1NF substrate bound and chose fifteen residues for optimization (figs. S10, S11, S13, and S14). These residues primarily reside in three regions: the C-terminal, α helix, and β barrel of the C-terminal domain, as well as in loops surrounding the active site (Fig. 2A). We have also established a high-throughput screening (HTS) platform based on copper-catalyzed azide-alkvne cycloaddition (CuAAC) (18) and achieved reliable quantification of enzymatic azidation products with a coefficient of variation of 9% and a detection limit of 4 μM (scheme S1 and fig. S2). With this HTS platform, we evaluated more than 5000 clones generated through error-prone polymerase chain reaction (PCR) or site-saturation mutagenesis (Fig. 2, B and C). A sextuple mutant Sav HppD V189A F216A P243A N245Q Q255A L367I (denoted as Sav HppD Az1) furnished the product with 1340 TTN and 87:13 e.r. In this evolution campaign, we could not identify an enzyme variant with an e.r. higher than 87:13. This result indicates that mutations that were beneficial for improving activity might not necessarily lead to an increase in enantioselectivity, which might be due to the differences in substrate positioning and geometric requirements for the rate-determining

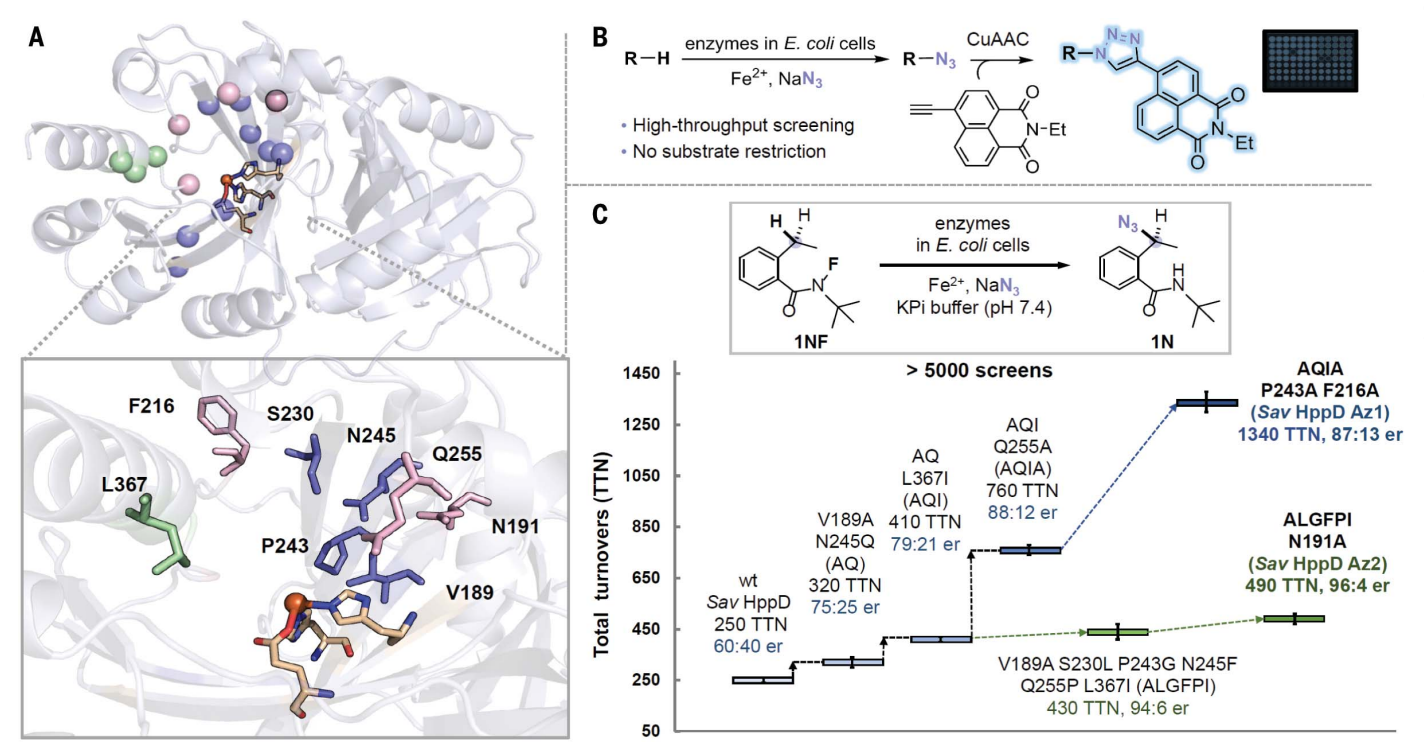


Fig. 2. Directed evolution of nonheme iron enzymes for radical–relay C–H azidation. (**A**) Protein residues selected for mutagenesis. Pink: loop residues surrounding the active site (N191, F216, Q255, and F359); green: residues on the C-terminal α helix (K361, L367, and N363); blue: residues on the β barrel of the C-terminal domain (V189, S230, P243, N245, Q269, Q334, F336, and R353) (PDB: 1T47). (**B**) A high-throughput screening platform for detection of

enzymatic azidation products. (**C**) Representative variants identified during the directed evolution of *Sav* HppD. Experiments were performed at the analytical scale by using suspensions of *Escherichia coli* (*E. coli*) cells expressing *Sav* HppD variants (OD $_{600}$ = 10), 10 mM substrate **1NF**, 25 mM NaN $_3$, 2.5 mM Fe $^{2+}$ in KPi buffer (pH 7.4) at room temperature under anaerobic conditions for 24 hours (table S2).

Rui et al., Science **376**, 869–874 (2022) 20 May 2022 **2 of 6**

N-F activation step and the enantio-determining azide rebound step as revealed by molecular dynamics (MD) simulation (fig. S18). In this regard, we reevaluated some of the libraries with chiral HPLC and performed additional rounds

of evolution aided by computational modelling (for details see figs. S13 and S14). We found a septuple mutant Sav HppD V189A N191A S230L P243G N245F Q255P L367I (denoted as Sav HppD Az2) that showed an enantio-

selectivity of 96:4 e.r. and 490 TTN. Kinetic analyses with purified enzymes showed that the Az1 variant exhibited a 4.1-fold increase in $k_{\rm cat}$ and a 1.7-fold increase in $K_{\rm M}$ over the WT enzyme [29.4 min⁻¹ (Az1) versus 7.20 min⁻¹

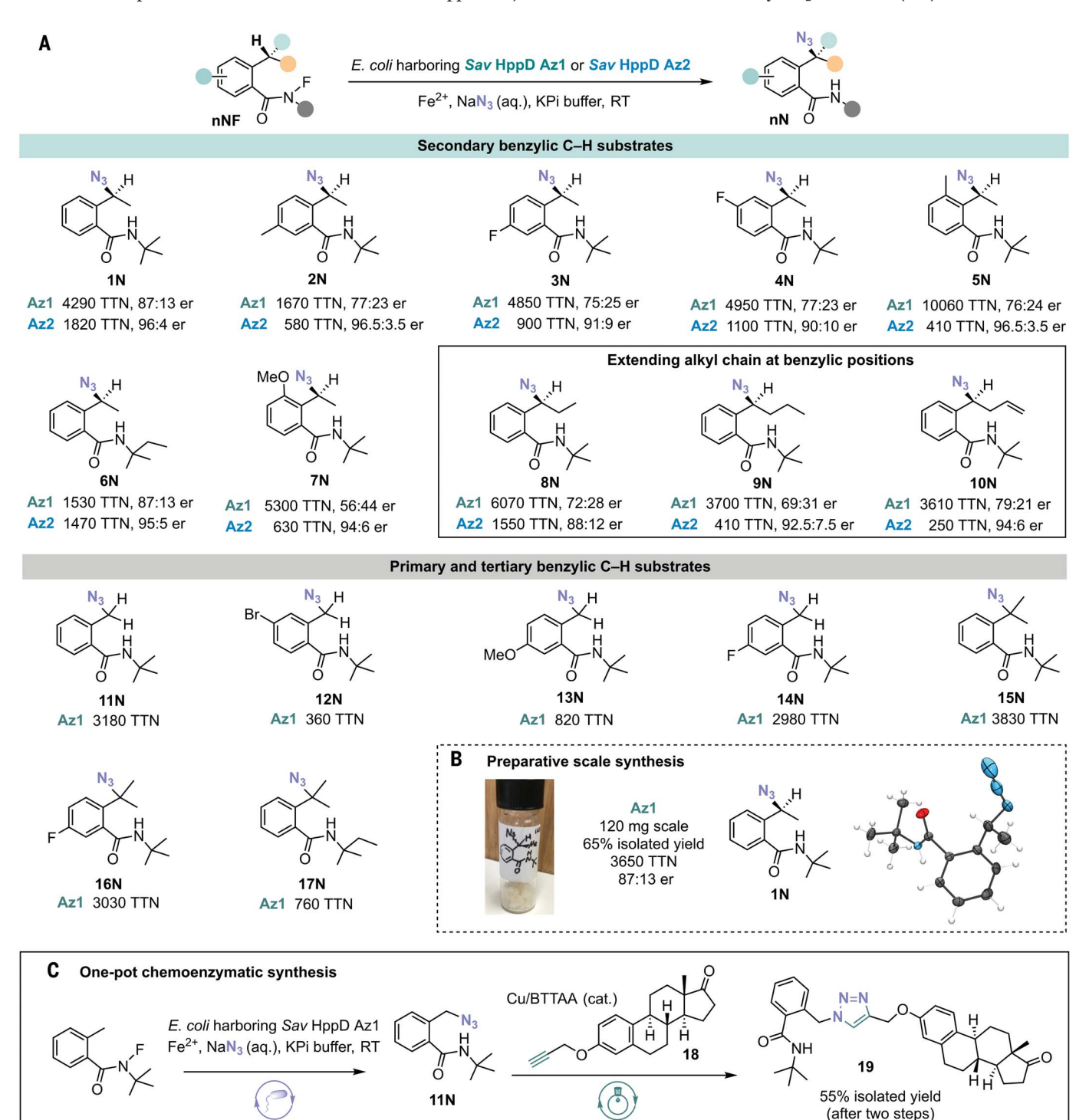


Fig. 3. Substrate scope and synthetic applications of enzymatic C–H azidation via iron-catalyzed radical relay. (A) Substrate scope of *Sav* HppD Az1 and *Sav* HppD Az2. Experiments were performed at the analytical scale by using suspensions of *E. coli* expressing *Sav* HppD variants in the KPi buffer (pH 7.4) at room temperature under anaerobic conditions for 24 hours (for detailed conditions see table S3). The absolute configuration of enzymatically

synthesized azidation product **1** was determined to be *S* through x-ray crystallography. The absolute configurations of all other azidation products were inferred by analogy. (**B**) Preparative scale synthesis and absolute configuration determination. (**C**) One-pot chemoenzymatic synthesis by in situ derivatization of enzymatic azidation products through CuAAC (for detailed conditions see section IX of the supplementary materials).

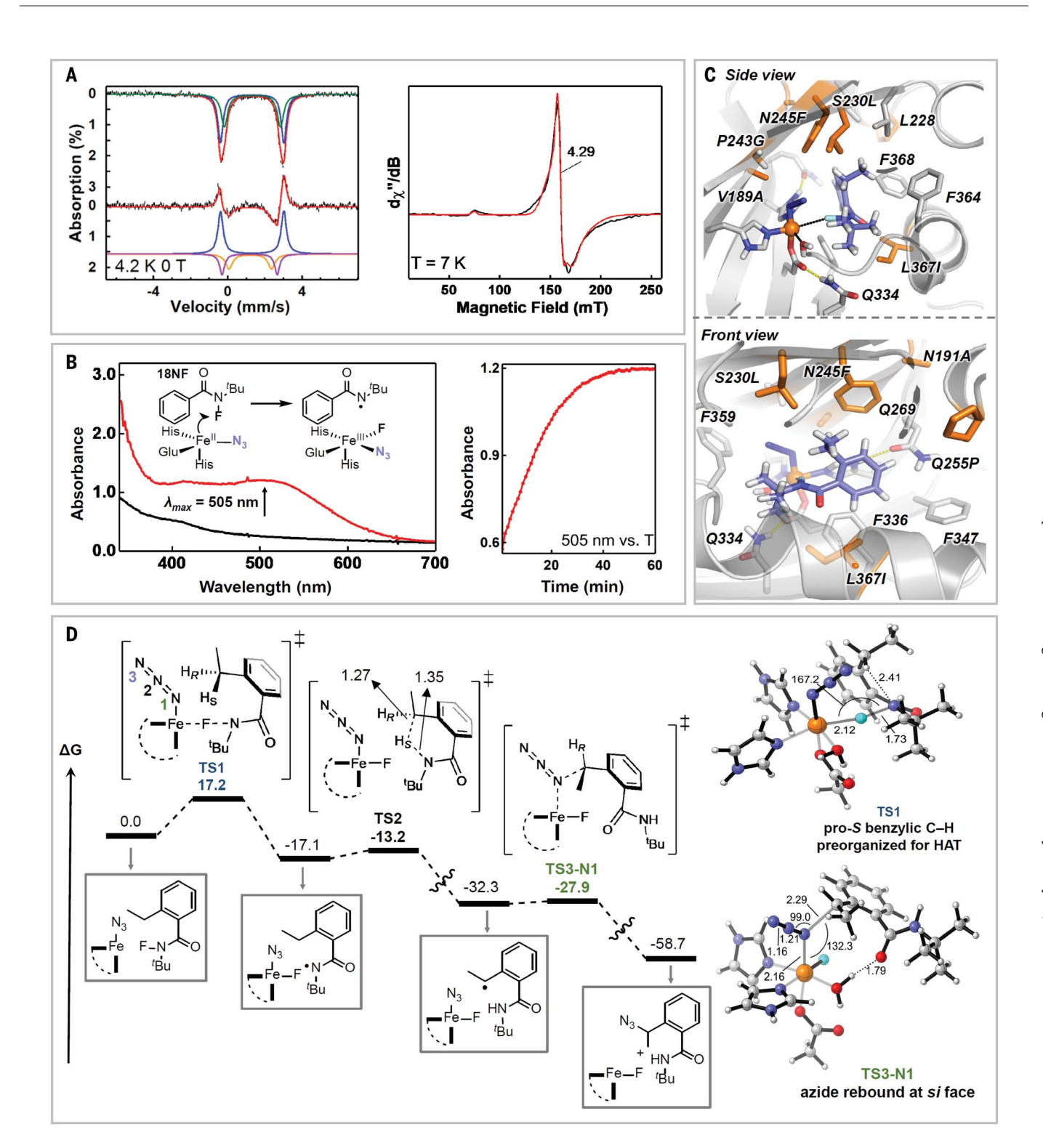


Fig. 4. Spectroscopic and computational studies of the enzymatic radical-relay C-H azidation. (A) (Left) Mössbauer spectrum of the Sav HppD Az1•Fe(II) complex (top, black) and the spectroscopic changes upon azide addition (bottom, black). The upward and downward absorption peaks represent the spectral components that disappeared or appeared, respectively, after the addition of azide. The colored solid lines represent spectral simulations (see supplementary materials for detailed discussion). (Right) EPR spectrum of Sav HppD Az1•Fe(II)•N₃ complex after incubation with **18NF** for 60 min (black) and the spectral simulation (red). (B) (Left) Optical absorption spectra

of Sav HppD Az1•Fe(II)•N $_3$ complex with **18NF** (black) and after incubation with **18NF** for 60 min (red). The inset shows the reaction scheme. (Right) The time-dependent change in the 505 nm feature. (**C**) Active site arrangement of the Az2 variant with **1NF** substrate bound in a near-attack conformation for N–F activation characterized from MD simulations (see supplementary materials for details; fig. S15). (**D**) Reaction mechanism obtained from DFT calculations employing a truncated active-site model built from MD simulations (see fig. S18 for details) (energies in kcal/mol, distances in Å, and angles in degrees).

(wild type) for $k_{\rm cat}$ and 790 μM (Az1) versus $470 \,\mu\text{M}$ (wild type) for K_{M}], whereas the more enantioselective Az2 variant displayed a 9-fold decrease in $k_{\rm cat}$ (3.39 min⁻¹) and a 6.6-fold decrease in $K_{\rm M}$ (120 $\mu{\rm M}$). Overall, both variants showed ~2-fold improvement in catalytic efficiency $(k_{cat}/K_{\rm M})$ compared with that of the WT enzyme (fig. S3).

With these two final variants in hand, we optimized reaction conditions (table S3) and assayed a range of N-fluoroamide substrates to explore the scope and limitation of this reaction (Fig. 3A). Sav HppD Az1 generally exhibited higher activity but lower enantioselectivity than Sav HppD Az2. The enzymatic reaction tolerated a range of aromatic substitution patterns with total turnovers up to 10,060 and enantiomeric ratio up to 96.5:3.5 (product 5N). Substrates with an extended alkyl chain at the benzylic position were well tolerated, providing products with moderateto-good TTNs and enantioselectivity (products **8N** to **10N**). The amide nitrogen substituent also affected enzyme performance as evidenced by a decrease in activity when a larger N-tertamyl group is substituted for the N-tert-butyl group (1N and 6N, 15N and 17N). We also tried to extend the scope of N-radical precursors and replace azide with another halide or pseudohalide anion (scheme S2 and table S4). However, these efforts have not been successful as starting materials were recovered in most cases. As suggested by Mössbauer studies, the inability of our method to incorporate other anionic ligands might be due to much weaker binding of these anions to the Fe(II) center of the enzymes. In a larger-scale reaction, Sav HppD Az1 furnished 1N in 65% isolated yield at a 120-mg scale with undiminished enantioselectivity (Fig. 3B). We also obtained single crystals of 1N and assigned their absolute configuration as S by x-ray crystallography. We also produced primary organic azide 11N at a preparative scale and subsequently converted it into the estrone derivative 18 through a CuAAC reaction (Fig. 3C). This chemoenzymatic two-step synthesis yielded the triazole product 19 in 55% isolated yield, demonstrating the potential of our platform to produce highly functionalized molecules when used in tandem with biocompatible reactions.

We conducted several mechanistic studies to investigate the catalytic cycle proposed in Fig. 1C. Addition of N₃⁻ to the Sav HppD Az1. Fe(II) complex induced the formation of two quadrupole doublets in the Mössbauer spectrum with isomer shifts (δ) of 1.20 and 1.17 mm/s and quadrupole splittings (ΔE_Q) of 2.29 and 2.97 mm/s, respectively. The observation of two quadrupole doublets may reflect different azide binding configurations to the Fe(II) center (Fig. 4A and figs. S5, S8, and S10; see section X of the supplementary materials for further discussion). We then carried out

electron paramagnetic resonance (EPR) measurements on a nitric oxide (NO)-bound Sav HppD Az1. Fe(II) complex, which has a prominent g ~ 4 EPR resonance that can be used to monitor the interactions between the substrate and the nonheme iron center (19). Adding azide to the Sav HppD Az1•Fe(II)•NO complex increased the rhombicity (E/D) of the g ~ 4 signal from 0.014 to ~0.017, and further addition of **1NF** continued the increase in the signal rhombicity (E/D = 0.023). These observations suggest that both N_3 and $\mathbf{1NF}$ interact with the Fe(II) center of Sav HppD Az1 (Fig. 4A, fig. S7, and table S6). To demonstrate that an Fe(III)-N₃ species is involved in the reaction, we incubated Sav HppD Az1•Fe(II)•N₃ with an N-fluoroamide 18NF that lacked the reactive benzylic C-H bonds. Slow accumulation of a red species was observed by optical absorption centered at 505 nm (Fig. 4B), which likely originated from the Fe(III)-N₃ ligand-to-metal charge transfer band (20-22). The EPR signal of this red species was located at g ~ 4.3, further confirming that the iron oxidation state of the formed species is in high spin (S = 5/2) Fe(III) (see section X of the supplementary materials). We also observed the formation of a minor stable organic radical centered at g = 2(scheme S6). Although further studies are needed to characterize this radical species, we speculated that it may be a secondary radical formed through quenching of the initial amidyl radical, as this g = 2 signal was not observed when incubating Sav HppD Az1•Fe(II)•N₃ with the model N-fluoroamide substrate **1NF** (scheme S6).

We also performed computational modelling to understand the molecular basis of this reaction. Focusing on enantioselective variant Sav HppD Az2, MD simulations showed that V189A and P243G generated more space to accommodate iron-bound azide in the active site (Fig. 4C and figs. S8 to S12). In WT Sav HppD, N191, N245, and S230 participated in a hydrogen bonding network with Q269 for native substrate positioning (23). Introduction of the mutations N191A, S230L, and P243G disrupted this network. These mutations, together with N245F and L367I, created a hydrophobic environment to accommodate N-fluoroamide substrate 1NF for N-F activation and position the ethyl group of the substrate closer to the iron-bound azide in a restricted and preorganized conformation for the subsequent reaction steps (Fig. 4C and fig. S18). Model DFT calculations (Fig. 4D) indicated that the initial N-F activation step ($\Delta G^{\ddagger}(TS3-N1) = 17.2 \text{ kcal}$ · mol⁻¹) was rate limiting and was followed by a fast 1,5-HAT ($\Delta G^{\ddagger}(TS2) = 3.9 \text{ kcal·mol}^{-1}$) to the N-centered radical. This mechanistic scheme was similar to that reported in an iron-catalyzed fluoroamide-directed fluorination (24) and was consistent with the absence of a kinetic isotope effect through measuring independent initial rates for reactions with **1NF** and **1NF**- d_2 (fig. S4). The major conformation of substrate **1NF** in Az2 preorganized the pro-S benzylic C-H bond for HAT, with the benzylic carbon projected in proximity to the iron-bound azide (Figs. 4C and fig. S18). Therefore, after 1,5-HAT the resulting C-radical was well positioned for azide recombination in a stereo-retentive manner with low energy barriers ($\Delta G^{\ddagger}(TS3-$ N1) = 4.4 kcal·mol⁻¹). Notably, although fluorine transfer had an intrinsically low activation barrier ($\Delta G^{\ddagger} = 5.0 \text{ kcal·mol}^{-1}$, fig. S18), steric constraints imposed within the active site likely prevented the substrate repositioning to enable fluorine recombination. Such control of radical rebound through substrate positioning has also been observed in native reactions catalyzed by nonheme iron halogenases, in which the proximity of substrate radicals toward the iron-bound chloride facilitated C-Cl bond formation over C-OH bond formation (25, 26).

The biocatalytic system reported here performs C(sp³)-H functionalization reactions through a metal-catalyzed radical-relay mechanism, thus expanding the scope of nonheme iron enzyme catalysis. We envision that the merger of various radical generation processes in synthetic chemistry and the capability of metalloenzymes for radical trapping will provide a powerful and general strategy to advance the frontier of radical biocatalysis.

REFERENCES AND NOTES

- F. H. Arnold, Angew. Chem. Int. Ed. 57, 4143-4148 (2018)
- U. T. Bornscheuer, Philos. Trans. R. Soc. A 376, 20170063 (2018).
- K. Chen, F. H. Arnold, Nat. Catal. 3. 203-213 (2020). O. F. Brandenberg, R. Fasan, F. H. Arnold, Curr. Opin.
- Biotechnol. 47, 102-111 (2017).
- K. F. Biegasiewicz et al., Science 364, 1166-1169 (2019).
- X. Huang et al., Nature 584, 69-74 (2020).
- P. Ji, J. Park, Y. Gu, D. S. Clark, J. F. Hartwig, Nat. Chem. 13, 312-318 (2021).
- L. M. Stateman, K. M. Nakafuku, D. A. Nagib, Synthesis 50, 1569-1586 (2018).
- C. Zhang, Z.-L. Li, Q.-S. Gu, X.-Y. Liu, Nat. Commun. 12, 475 (2021). F. Wang, P. Chen, G. Liu, Acc. Chem. Res. 51, 2036–2046 (2018).
- 11. B. J. Groendyke, D. I. AbuSalim, S. P. Cook, J. Am. Chem. Soc. **138** 12771-12774 (2016)
- C. Crowe et al., Chem. Soc. Rev. 50, 9443-9481 (2021).
- 13. M. L. Matthews et al., Nat. Chem. Biol. 10, 209-215 (2014) 14. M. E. Neugebauer et al., Nat. Chem. Biol. 15, 1009-1016 (2019).
- 15. C. Y. Kim et al., Nat. Commun. 11, 1867 (2020).
- 16. X. Huang, J. T. Groves, J. Biol. Inorg 22, 185-207 (2017)
- P. Sivaguru, Y. Ning, X. Bi, Chem. Rev. 121, 4253-4307 (2021).
- 18. M. Meldal, C. W. Tornøe, Chem. Rev. 108, 2952-3015 (2008).
- 19. A. M. Orville et al., Biochemistry 31, 4602-4612 (1992).
- 20. C. Bull, J. A. Fee, J. Am. Chem. Soc. 107, 3295-3304 (1985)
- 21. K. Meyer, E. Bill, B. Mienert, T. Weyhermüller, K. Wieghardt, J. Am. Chem. Soc. 121, 4859-4876 (1999).
- 22. C. A. Grapperhaus, B. Mienert, E. Bill, T. Weyhermüller, K. Wieghardt, Inorg. Chem. 39, 5306-5317 (2000).
- 23. J. M. Brownlee, K. Johnson-Winters, D. H. T. Harrison, G. R. Moran, Biochemistry 43, 6370-6377 (2004).
- 24. E. N. Pinter, J. E. Bingham, D. I. AbuSalim, S. P. Cook, Chem. Sci. 11, 1102-1106 (2020).
- 25. M. L. Matthews et al., Proc. Natl. Acad. Sci. U.S.A. 106, 17723-17728 (2009).
- 26. L. C. Blasiak, C. L. Drennan, Acc. Chem. Res. 42, 147-155 (2009).

ACKNOWLEDGMENTS

We thank M. Greenberg for helpful discussion and comments on the manuscript. We thank M.A. Siegler and the JHU X-ray Crystallography Facility for analytical support. We also thank K. Tripp and the JHU Center for Molecular Biophysics (CMB) for assistance in performing the CD experiments. Funding: Financial support was provided by the Johns Hopkins University, the David and Lucile Packard Foundation, and National Institute for General Medical Sciences ROOGM129419 (to X.H.). Y.G. is thankful for financial support from the National Science Foundation, CHE1654060. This work was also supported by the Generalitat de Catalunya AGAUR Beatriu de Pinós H2020 MSCA-Cofund 2018-BP-00204 project (to M.G.B.), the Spanish MICINN (Ministerio de Ciencia e Innovación) PID2019-111300GA-I00 project (to M.G.B.) and the Ramón y Cajal program via the RYC2020-028628-I fellowship (to M.G.B.), and the Spanish MIU (Ministerio de Universidades) predoctoral fellowship FPU18/02380 (to J.S.). Author contributions: X.H. conceived and directed the project. X.H., J.R., and Q.Z. designed the experiments. J.R. performed the screening of the initial enzyme activity. X.H. and A.J.H. developed the high-throughput screening platform. J.R., Q.Z., and A.J.H. performed the directed evolution and results analyses. J.R., Q.Z., V.R., and Z.C. performed the substrate scope study. J.C.P. carried out the spectroscopic studies with Y.G.

providing guidance. M.G.B. conceived and directed the computational modelling studies. J.S. and M.G.B. performed the MD simulations. J.S., Y.Y., and M.G.B. performed the DFT calculations. X.H. and J.R. wrote the manuscript with input from all other authors, M.G.B. wrote the computational sections. Competing Interests: A provisional patent application covering enantioselective biocatalytic C-N₃ bond formation has been under preparation and will be filed through the Johns Hopkins University with J.R., Q.Z., X.H., A.J.H., and Z.C. as inventors. Authors J.S., J.C.P., V.R., Y.Y., Y.G., and M.G.B. declare no competing financial interests. Data and materials availability: All data needed to evaluate the conclusions in this study are present in the main paper or in the supplementary materials. The crystal structure of **1N** is available from the Cambridge Crystallographic Data Centre under reference number CCDC 2163783. License information: Copyright © 2022 the authors, some rights reserved; exclusive licensee American Association for the Advancement of

Science. No claim to original US government works. https://www.sciencemag.org/about/science-licenses-journal-article-reuse

SUPPLEMENTARY MATERIALS

science.org/doi/10.1126/science.abj2830 Materials and Methods Figs. S1 to S20 Schemes S1 to S6 Tables S1 to S9 References (27–61)

View/request a protocol for this paper from Bio-protocol.

Submitted 2 May 2021; resubmitted 14 January 2022 Accepted 14 April 2022 10.1126/science.abj2830

Rui et al., Science **376**, 869-874 (2022) 20 May 2022 **6 of 6**



Directed evolution of nonheme iron enzymes to access abiological radical-relay C(sp³)-H azidation

Jinyan Rui, Qun Zhao, Anthony J. Huls, Jordi Soler, Jared C. Paris, Zhenhong Chen, Viktor Reshetnikov, Yunfang Yang, Yisong Guo, Marc Garcia-Borrs, and Xiongyi Huang

Science, 376 (6595), .

DOI: 10.1126/science.abj2830

Adapting iron enzymes for azidation

Nonheme iron enzymes typically activate molecular oxygen to initiate oxidation of a substrate or atom transfer through radical mechanisms. Rui *et al.* used directed evolution to encourage a nonheme iron oxidase to perform enantioselective azide transfer using an aryl *N*-fluoroamide as both substrate and radical initiator. The resulting azides, installed on an ortho alkyl group, may be useful starting points for synthesis or handles for bioorthogonal coupling. — MAF

View the article online

https://www.science.org/doi/10.1126/science.abj2830

Permissions

https://www.science.org/help/reprints-and-permissions

Use of this article is subject to the Terms of service